A Command Shaping Approach for Suppressing Scattered Responses on Servo Systems with Rolling Friction

Yoshihiro Maeda and Makoto Iwasaki

***Abstract*— This paper presents a novel command shaping approach which aims at suppressing scattered responses due to rolling friction, for the fast and precise sequential positioning control with micrometer-stroke. The concept of the proposed command shaping is to prevent an overshoot response which leads to the scattered responses, considering the complicated and nonlinear rolling friction behavior. The command shaping filter design presented in this study is friction-model-free and is based on the constrained optimization framework. The effectiveness of the proposed approach is demonstrated through experiments for a laboratory table positioning system.**

I. Introduction

Industrial mechatronic systems such as electronics manufacturing machines are subjected to friction forces, e.g., rolling friction generated at linear guides and bearings with rolling elements, which deteriorate fast-response and high-precision positioning performance [1], [2]. In recent years, for demands of higher density in processing objects, the positioning stroke is getting shorter (micrometer-stroke), and the micrometer-stroke point-to-point motion is sequentially and repetitively performed (so-called "inching motion") [3]. However, the rolling friction generally shows nonlinear elastic behavior in the micrometer-stroke motion, which causes scattered position responses among the sequential positioning trials. Hence, effective friction compensation techniques are required for the fine micrometer-stroke sequential motion.

In the research fields on friction compensation, most of friction compensation techniques are the friction-model-based approach such as model-based feedforward (FF) friction compensation in combination with linear feedback (FB) control strategies (e.g., PID and disturbance observer) [4], [5], [6], because of the fine compensation performance for the rolling friction behavior. A precise friction model is indispensable in order to acquire ideal friction cancellation, while complicated-structure friction models and/or friction compensation algorithms are necessary, which may lead to increase of labor on the compensation design and computation loads on on-line calculation [1], [7].

On the other hand, the friction-model-free approach such as learning control [2], [8], disturbance observer [4], sliding mode control [9], etc., compensates for the nonlinear friction phenomena without information of friction. However, the friction compensation ability is restricted by instability of the control system and is deteriorated in comparison to the precise-friction-model-based FF approach. Hence, it is better to use the friction-model-free approach in combination with the friction-model-based FF approach [1].

*This work was supported by Via Mechanics, Ltd.

Yoshihiro Maeda and Makoto Iwasaki are with the Department of Electrical and Mechanical Engineering, Nagoya Institute of Technology, Gokiso, Showa, Nagoya, 4668555, Japan ymaeda@nitech.ac.jp

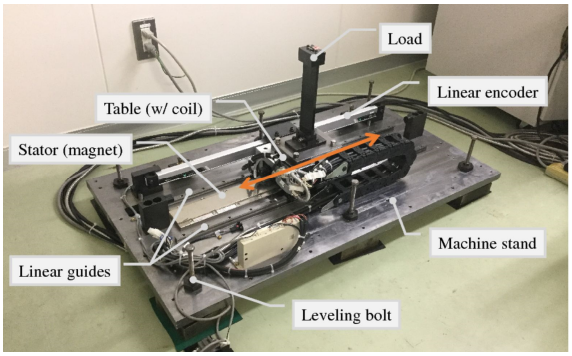

Fig. 1. Linear motor-driven table as laboratory prototype.

This paper presents a novel friction-model-free position command shaping approach for suppressing the scattered responses in the fast and precise micrometer-stroke positioning motion, which has never been examined in literature. The proposed approach generates a position trajectory reference aiming at suppressing an overshoot response in each positioning trial through a command shaping filter. The command shaping filter is designed based on constrained optimization, with consideration of rolling friction properties in macro- and micro-displacement regions (friction-model-free). The proposed command shaping approach does not affect to stability of position control systems applied and can be used with the conventional friction-model-based and/or friction-model-free friction compensation approaches. The effectiveness of the proposed approach is verified in combination of the friction-model-based FF compensation and the PID linear FB control, through experiments using a laboratory linear motor-driven table positioning device.

II. Servo System with Rolling Friction

A. Linear motor-driven table

Fig. 1 shows the exterior of the prototype table positioning system for electronics manufacturing machines, machine tools, etc. A moving table on a machine stand is driven by an AC linear motor along rolling-ball linear guides, where rolling friction is generated. A mass load is mounted on the table through a flexible beam and has a resonant mode of about 81 Hz. On the other hand, the machine stand supported by six leveling bolts on the floor also causes resonant vibration of about 38 Hz. A linear encoder along the

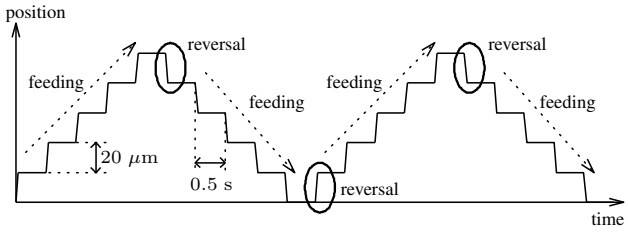

Fig. 2. Test pattern of sequential positioning motion.

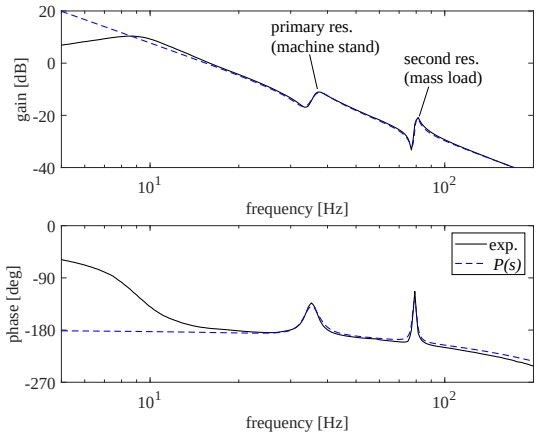

Fig. 3. Bode plots of table position for motor thrust reference.

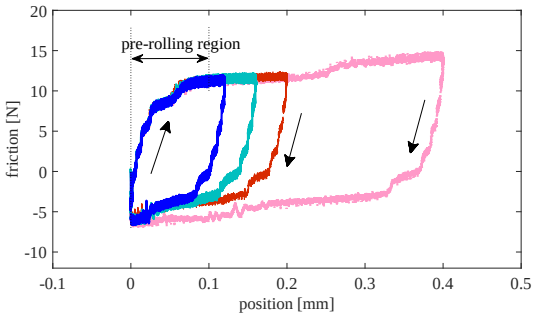

Fig. 4. Rolling friction characteristics.

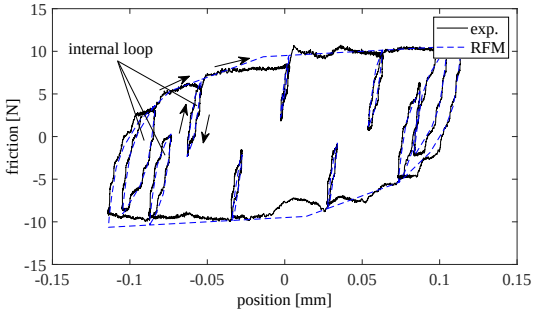

Fig. 5. Rolling friction characteristics.

guides detects the table position, and the detected position is controlled in a full-closed position control manner through a DSP (SDS, PCI-DSP46713, sampling time of 500 μs) and an AC servo amplifier (Sanyo Denki, PY0, current control bandwidth of about 750 Hz).

B. Target control specification

The sequential positioning motion (inching motion) shown in Fig. 2 is evaluated in this study, with consideration of a typical motion pattern in industry. Each point-to-point positioning motion is performed with stroke of $Y_r = 20$ μm and the interval time of 0.5 s. The actual position should follow to the target position with the accuracy of ± 2 μm by the settling time of 35 ms in each positioning trial.

C. Frequency response characteristic

Dark solid lines in Fig. 3 indicate an experimental Bode plot of the detected table position y for the motor thrust reference u as control input. There are two resonant modes at 38 Hz and 81 Hz owing to the flexible mass load and the machine stand. In addition, the current control system and low-pass filters in the servo amplifiers address a phase delay property as shown in the high frequency range.

A linear plant model $P(s) = y(s)/u(s)$ can be defined by

$$P(s) = C_d(s) \cdot K_t \left(\frac{k_0}{s^2} + \sum_{i=1}^{2} \frac{k_i}{s^2 + 2\zeta_i \omega_i s + \omega_i s^2} \right), \quad (1)$$

where $C_d(s)$ is the phase delay model, K_t is the motor thrust constant, ω_i is the natural angular frequency of the i-th vibration mode, ζ_i is the damping coefficient, and k_i is the vibration mode gain, respectively. Dark broken lines in Fig. 3 depict a Bode plot of $P(s)$. Note that model errors at the low frequencies less than 20 Hz are the influence of the nonlinear friction, which can be modeled by introducing a precise friction model (see [1], [7] for details).

D. Rolling friction characteristic

Figs. 4 and 5 show rolling friction characteristics of the experimental device. From Fig. 4, the rolling friction reveals the nonlinear elastic property in the micro-displacement region (so called "pre-rolling region"), and the pre-rolling region is about 100 μm. On the other hand, as indicated by a dark solid line in Fig. 5 which includes several internal loops, the elastic friction property suddenly varies when the friction trajectory in an internal loop returns to the outer loop. That is, the rolling friction behaves depending on history of the past position trajectory (so-called "history dependency" or "memory characteristic") [1], [3], [4].

For analysis and compensation of the rolling friction during the fine positioning motion, a multi-structure rolling friction model [7] ("RFM" in the following) shown in Fig. 6 is introduced in this study. In Fig. 6, f_{roll} is the rolling friction force as output, x is the position corresponding to y as input, $f_j (j = 1, \ldots, M)$ is the element force, x_j is the element position, F_{mj} is the maximum element force, K_j is the element elastic coefficient, and D_j is the element viscous coefficient, respectively. f_{roll} is calculated as (2), by summing all the elementary models' outputs.

$$f_{roll} = \sum_{j=1}^{M} f_j \quad (2)$$

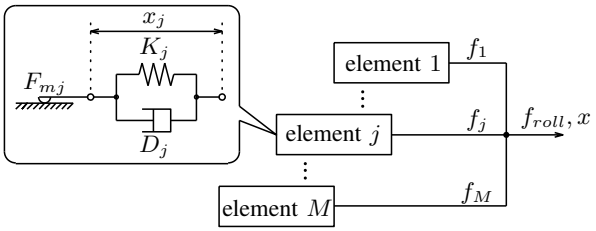

Fig. 6. Conceptual diagram of rolling friction model.

The parameters K_j, D_j, and F_{mj} are identified through Back Propagation algorithm with $M = 10$, by giving experimental data such as Figs. 4 and 5 to the algorithm as teaching data (see [7] for more detail).

Dark broken line in Fig. 5 indicates the history dependency of RFM, which well-reproduces the actual rolling friction.

III. Scattered Responses in Sequential Positioning Motion

A. Position control system using friction-model-based FF friction compensation and linear FB compensation

Fig. 7 shows a block diagram of a two-degree-of-freedom (2DoF) table position control system, where $F_{cs}(z)$ is the command shaping filter based on the deadbeat FF control framework [10], $P_{ff}(z)$ is the discrete plant model of (1), $C_d(z)$ is the phase delay compensator as the discrete model of $C_d(s)$ in (1), $C_{fb}(z)$ is the PID-type linear FB controller, r_c is the position command with amplitude of Y_c (step signal), r_t is the target position trajectory, u_{ff} is the FF motor thrust reference, and f_{roll} is the FF friction compensation force generated by RFM, respectively.

$C_{fb}(z)$ is designed so that the FB control system possess a higher control bandwidth as much as possible (gain-cross frequency is about 60 Hz) under the specified stability margins (gain margin of 5 dB and phase margin of 30 deg). The RFM-based FF friction compensation performs delay-free compensation by using the position trajectory $F_{cs}(z)r_c(z)$ as input to RFM, aiming at friction cancellation during the positioning motion.

B. Design method of conventional command shaping filter

Fig. 8 shows a block diagram of the FF control system in Fig. 7 for the design of the command shaping filter $F_{cs}(z)$. Note that if the plant model $P_{ff}(z)$ for the design of $F_{cs}(z)$ reproduces the actual plant $P(z)$, $r_t(s) = y(s)$ can be realized. Hence, $P(z) = P_{ff}(z) = N_P(z)/D_P(z)$ is assumed in the following design. The transfer function of $F_{cs}(z)$ is formulated by (3), as an N-th order FIR filter with a free parameter vector $\boldsymbol{\rho} \in \mathbb{R}^{N+1}$:

$$F_{cs}(z) = \frac{N_{cs}(z)}{z^N} = \frac{[z^N \cdots z\ 1]\boldsymbol{\rho}}{z^N}, \qquad \boldsymbol{\rho} = [\rho_N\ \cdots\ \rho_1\ \rho_0]^T. \tag{3}$$

In order to achieve the point-to-point positioning motion with the specified settling time, $\boldsymbol{\rho}$ is designed in consideration of the following two equality constraints.

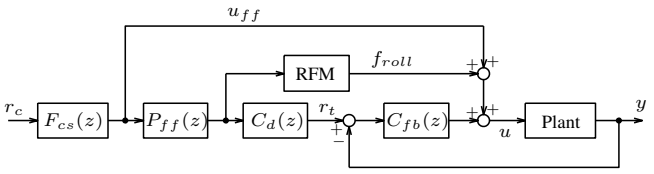

Fig. 7. Block diagram of position control system with command shaping filter.

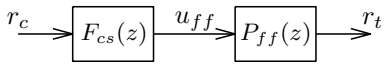

Fig. 8. Block diagram of FF control system.

a) Pole-zero cancellation: the transfer characteristic $r_t(s)/r_c(s)$ in Fig. 8 is expressed as

$$\frac{r_t(z)}{r_c(z)} = P_{ff}(z)F_{cs}(z) = \frac{N_P(z)}{D_P(z)}\frac{N_{cs}(z)}{z^N}. \tag{4}$$

In order to settle r_t to r_c (step signal) by $N+1$ steps, $N_{cs}(z)$ has to include all roots λ_l $(l = 1, 2, \ldots, N_\lambda)$ of $D_P(z)$. The mathematical expression is given by

$$\begin{aligned} N_{cs}(\lambda_l) &= \rho_N\lambda_l^N + \cdots + \rho_1\lambda_l + \rho_0 \\ &= [\lambda_l^N\ \cdots\ \lambda_l\ 1]\boldsymbol{\rho} = 0. \end{aligned} \tag{5}$$

Thus, the equality constraint is defined as

$$\boldsymbol{\Theta}_a\boldsymbol{\rho} = \boldsymbol{\Gamma}_a, \tag{6}$$

where $\boldsymbol{\Theta}_a \in \mathbb{C}^{N_\lambda \times (N+1)}$ and $\boldsymbol{\Gamma}_a \in \mathbb{R}^{N_\lambda}$ are given by

$$\boldsymbol{\Theta}_a = \begin{bmatrix} \lambda_1^N & \cdots & \lambda_1 & 1 \\ \lambda_2^N & \cdots & \lambda_2 & 1 \\ \vdots & \vdots & \vdots & \vdots \\ \lambda_{N_\lambda}^N & \cdots & \lambda_{N_\lambda} & 1 \end{bmatrix},\ \boldsymbol{\Gamma}_a = [0 \cdots 0\ 0]^T.$$

b) Final-value theorem: The final-value of r_t for the step position command r_c is expressed as follows:

$$\begin{aligned} r_t(\infty) &= \lim_{z\to 1}(1 - z^{-1})\frac{N_P(z)}{D_P(z)}\frac{N_{cs}(z)}{z^N}r(z) \\ &= \frac{N_P(1)}{D_P(1)}\frac{N_{cs}(1)}{1}. \end{aligned} \tag{7}$$

In order to ensure the final-value theorem, i.e., $r_t(\infty) = 1$, the following condition should be satisfied.

$$N_{cs}(1) = \rho_N + \cdots + \rho_1 + \rho_0 = [1 \cdots 1\ 1]\boldsymbol{\rho} = \frac{D_P(1)}{N_P(1)} \tag{8}$$

Therefore, the equality constraint is expressed as

$$\boldsymbol{\Theta}_b\boldsymbol{\rho} = \Gamma_b, \tag{9}$$

where $\boldsymbol{\Theta}_b \in \mathbb{R}^{1\times(N+1)}$ and $\Gamma_b \in \mathbb{R}$ are given by

$$\boldsymbol{\Theta}_b = [1 \cdots 1\ 1],\ \Gamma_b = \frac{D_P(1)}{N_P(1)}.$$

On the other hand, an objective function J_{conv} which considers differential of the FF control input u_{ff} is defined

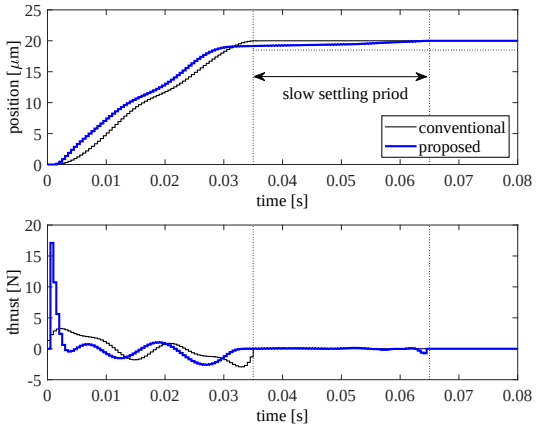

Fig. 9. Comparisons of position trajectory reference r_t and FF thrust u_{ff}.

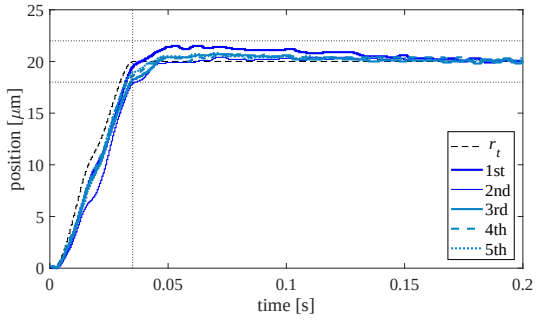

Fig. 10. Experimental results of conventional command shaping approach.

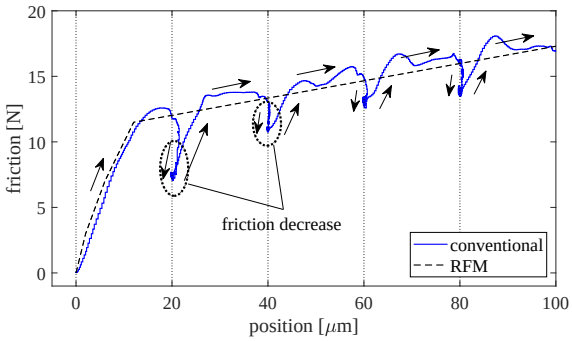

Fig. 11. Comparisons of estimated friction for table position.

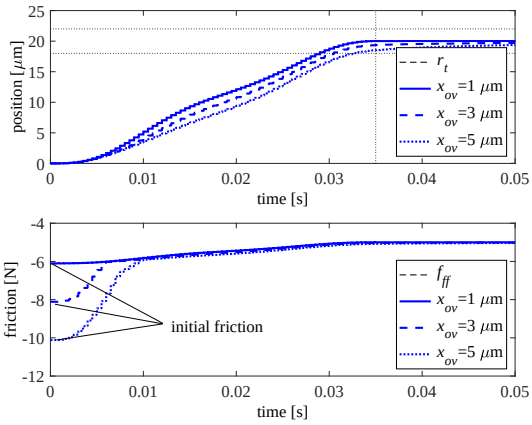

Fig. 12. Simulation results of table position and rolling friction under different overshoot displacement situations.

by (10), in order to generate the smooth trajectory r_t:

$$J_{conv} = \sum_{k=0}^{N} \left(u_{ff}[k] - u_{ff}[k-1]\right)^2 = \sum_{k=0}^{N} \rho_k^2 = \boldsymbol{\rho}^T \boldsymbol{\rho}, \quad (10)$$

where $u_{ff}[-1] = 0$. Note that the position stroke Y_r of r_c is assumed as $Y_r = 1$ in the objective function design.

Finally, the conventional command shaping filter is designed based on the following constrained optimization.

$$\begin{aligned} \min_{\boldsymbol{\rho}} \quad & J_{conv} \\ \text{s.t.} \quad & \boldsymbol{\Theta}_a \boldsymbol{\rho} = \boldsymbol{\Gamma}_a, \ \boldsymbol{\Theta}_b \boldsymbol{\rho} = \Gamma_b \end{aligned} \quad (11)$$

Optimization of (11) is performed according to the Lagrange multiplier method (see [10] for more detail).

C. Design of conventional command shaping filter

The conventional command shaping filter is designed with $N = 70$ in consideration of the target settling time of $35 (= 70T_s)$ ms. On the other hand, $P_{ff}(z)$ for the design of $F_{cs}(z)$ is assigned as the discrete-time plant model of (1).

Thin lines in Fig. 9 show response waveforms of r_t and u_{ff}. The shaped position trajectory r_t smoothly settles to $Y_r = 20$ μm by 35 ms.

D. Scattered responses and simulation analysis

Fig. 10 shows experimental response waveforms of the table position y in the sequential positioning motion as Fig. 2, where five response waveforms to positive direction are indicated. From the figure, the position responses implicitly scatter during the transient as well as at the settling region, which deteriorate the target settling accuracy of ± 2 μm.

In order to examine the friction behavior during the sequential motion, Lissajous waveforms of the friction force for y are indicated in Fig. 11, where a solid line is calculated by using the estimated friction force $\widehat{f}$ (by an off-line disturbance observer) and a broken line is calculated by using the FF friction compensation force f_{roll}, respectively. From the figure, $\widehat{f}$ and f_{roll} behave similar in each positioning trial and increase gradually by proceeding the positioning trial, since the rolling friction behaves mainly in the pre-rolling region in the micrometer-stroke motion [3]. However, the actual friction forces (i.e., $\widehat{f}$) at the settling region (around vertical dotted lines) decrease after the overshoot responses, and start from different friction forces in comparison with f_{roll}, which occurs remarkable friction compensation errors. The reference [7] has clarified that the friction decrease owns to the nonlinear elasticity of the rolling friction. Fig. 12 shows example simulation results of y and f_{roll} by intentionally giving the initial friction errors due to the overshoot x_{os} in the previous positioning trial. The initial friction errors cause the scattered responses in y during the transient, as same as the experimental results of Fig. 10.

In the conventional studies on the friction compensation, advanced friction-model-based and friction-model-free

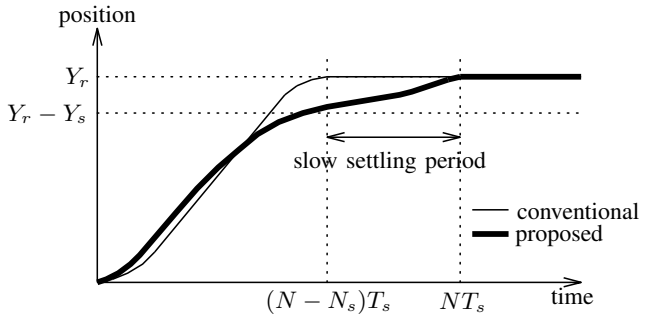

Fig. 13. Conceptual diagram of position trajectory.

friction compensation approaches are mainly presented, i.e., initial friction compensation [3], [7], combination of friction-model-based FF and linear FB [4], [5], [6], and nonlinear FB. In this study, a novel command shaping approach is examined in consideration of the rolling friction behavior in the sequential positioning motion.

IV. Proposed Command Shaping Approach Considering Rolling Friction

A. Command Shaping Strategy

Fig. 13 shows conceptual time-series waveforms of the position trajectory $r_t(= y)$ in the conventional and proposed command shaping approaches. The points of the proposed approach for preventing the overshoot response which causes the scattered responses are summarized as follows:

- The trajectory reference r_t is restricted to within $Y_r - Y_s < r_t < Y_r$ during the specified time period of $t = (N - N_s)T_s \sim (N-1)T_s$ ("slow settling period" in the following), and settles to the target position of Y_r at $t = NT_s$.
- The position trajectory reference r_t smoothly changes, specifically around the slow settling period.

By applying the shaped trajectory reference r_t to the position control system, the influence of the friction compensation errors and the other modeling errors is expected to be converged during the slow settling period while suppressing the overshoot response.

B. Design method of proposed command shaping filter

The proposed command shaping filter is designed based on constrained optimization in consideration of the conceptual position trajectory shown in Fig. 13.

• Inequality constraints for slow settling period: in order to restrict r_t during the slow settling period, the proposed method imposes the following inequality constraints to the design of $F_{cs}(z)$.

$$Y_r - Y_s < r_t[k] < Y_r \quad (k = N - N_s, \ldots, N-2, N-1) \tag{12}$$

Here, the shaped trajectory reference vector $\boldsymbol{R}_t \in \mathbb{R}^{N+1}$ is defined by (13) as a function of $\boldsymbol{\rho}$.

$$\boldsymbol{R}_t(\boldsymbol{\rho}) = [r_t[0]\ r_t[1] \cdots r_t[N]]^T = \boldsymbol{\Omega}_p \boldsymbol{R}_c \boldsymbol{\rho}, \tag{13}$$

where $\boldsymbol{\Omega}_p \in \mathbb{R}^{(N+1)\times(N+1)}$ and $\boldsymbol{R}_c \in \mathbb{R}^{(N+1)\times(N+1)}$ are defined as follows:

$$\boldsymbol{\Omega}_p = \begin{bmatrix} D_p & 0 & \cdots & 0 \\ \boldsymbol{C}_p\boldsymbol{B}_p & D_p & \cdots & 0 \\ \vdots & \vdots & \ddots & \vdots \\ \boldsymbol{C}_p\boldsymbol{A}_p^{N-1}\boldsymbol{B}_p & \boldsymbol{C}_p\boldsymbol{A}_p^{N-2}\boldsymbol{B}_p & \cdots & D_p \end{bmatrix},$$

$$\boldsymbol{R}_c = Y_r \begin{bmatrix} 1 & 0 & \cdots & 0 \\ 1 & 1 & \cdots & 0 \\ \vdots & \vdots & \ddots & \vdots \\ 1 & 1 & \cdots & 1 \end{bmatrix}.$$

By applying Schur complement, (12) can be transformed to the following LMI.

$$\boldsymbol{\Theta}_k(\boldsymbol{\rho}) = \begin{bmatrix} \bar{\Sigma} & \boldsymbol{E}_k\boldsymbol{Y}(\boldsymbol{\rho}) - \Sigma_0 \\ (\boldsymbol{E}_k\boldsymbol{Y}(\boldsymbol{\rho}))^T - \Sigma_0 & \bar{\Sigma} \end{bmatrix} > 0, \tag{14}$$

where $\boldsymbol{E}_k \in \mathbb{R}^{1\times(N+1)}$, $\bar{\Sigma} \in \mathbb{R}$, and $\Sigma_0 \in \mathbb{R}$ are given by

$$\boldsymbol{E}_l = [\ \underbrace{0\ \cdots\ 0\ 1}_{k}\ 0\ \cdots\ 0\ ],$$

$$\bar{\Sigma} = \frac{X_s}{2},\ \Sigma_0 = \frac{2X_r - X_s}{2}.$$

• Smoothing of settling trajectory: a new objective function J_{prop} which aims at smoothing the shaped trajectory r_t in the slow settling period is newly introduced as

$$\begin{aligned} J_{prop} &= \sum_{k=0}^{N} \{w_k\,(u_{ff}[k] - u_{ff}[k-1])\}^2 = \sum_{k=0}^{N} (w_k\rho_k)^2 \\ &= \boldsymbol{\rho}^T \boldsymbol{W}_s^T \boldsymbol{W}_s \boldsymbol{\rho}, \end{aligned} \tag{15}$$

where $u_{ff}[-1] = 0$, and $\boldsymbol{W}_s \in \mathbb{R}^{(N+1)\times(N+1)}$ is given by

$$\boldsymbol{W}_s = \mathrm{diag}(w_0, w_1, \cdots, w_N),\ w_k = \frac{K_w}{N}k + 1.$$

Therefore, by applying $K_w(> 0)$ to satisfy $w_{k-1} > w_k$, the smoothed trajectory reference $r_t[k]$ is generated around the slow settling period.

Finally, the proposed command shaping filter is designed by solving the following constrained optimization.

$$\begin{aligned} \min_{\boldsymbol{\rho}} \quad & J_{prop} \\ \text{s.t.} \quad & \boldsymbol{\Theta}_a\boldsymbol{\rho} = \boldsymbol{\Gamma}_a, \boldsymbol{\Theta}_b\boldsymbol{\rho} = \Gamma_b, \boldsymbol{\Theta}_k(\boldsymbol{\rho}) > 0 \end{aligned} \tag{16}$$

Since all the functions in (15) are expressed as Affine functions with respect to $\boldsymbol{\rho}$, (15) can be solved as a convex optimization problem based on the LMI technique.

C. Design of command shaping filter

In the proposed command shaping filter design, N, N_s, and Y_s are respectively set as $N = 130$, $N_s = 60$, and $Y_s = 1.5$ μm so that r_t almost settles to Y_r by the settling time of $35(= (N - N_s)T_s = 70T_s)$ ms. On the other hand, K_w is assigned as $K_w = 0.1$ in order to generate smooth r_t around the slow settling period. Although there are some additional parameters to the conventional approach, it is easy to set them.

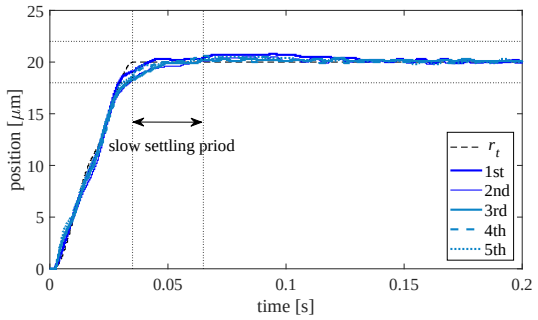

Fig. 14. Experimental results of proposed command shaping approach.

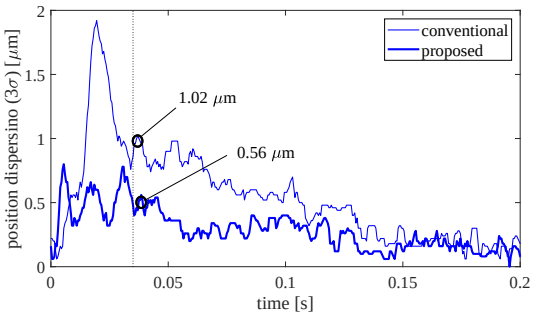

Fig. 15. Position dispersion in inching motion.

Bold lines in Fig. 9 indicate r_t and u_{ff} generated by the proposed command shaping filter. The shaped trajectory r_t is smoothed and has a margin to the target position of $Y_r = 20$ μm in the slow settling period for suppressing the overshoot response. However, as a contradiction of the objective function of (15) and the inequality constraints of (14), the initial thrust in u_{ff} is larger than the one of the conventional approach indicated by the thin line. Further improved filter design will be examined as the future challenges.

V. Experimental Evaluations

The sequential micrometer-stroke positioning motion is conducted by using the proposed command shaping filter. Note that the RFM for compensation as well as the FB controller $C_{fb}(z)$ are the same as of the experiments with the conventional command shaping filter in III-D.

Fig. 14 shows five experimental waveforms of y, while Fig. 15 shows the comparative position dispersion (3σ). From the figures, the proposed approach successfully reduces the maximum dispersion from 1.02 μm of the conventional approach to 0.56 μm (-45 %), and the target settling accuracy of ± 2 μm is satisfied only by shaping the position trajectory reference.

Table I lists the maximum overshoot displacement and its dispersion in the five-time positioning trials shown in Figs. 10 and 14. The proposed approach suppresses not only the maximum overshoot displacement but also the dispersion, which prevents the scattered responses, and the effectiveness of the proposed command shaping strategy presented in IV-A is verified.

TABLE I

Maximum overshoot displacement and its dispersion.

unit: μm

approach	max. overshoot displacement					avg.	dispersion
	1st	2nd	3rd	4th	5th		
conventional	1.5	0.4	0.7	0.7	0.8	0.82	1.10
proposed	0.8	0.5	0.4	0.6	0.5	0.56	0.41

VI. Conclusion

A novel command shaping approach for suppressing the scattered responses has been presented, and the effectiveness has been demonstrated through experiments using the linear motor-driven table system. The proposed command shaping is a friction-model-free scheme and can be combined with the conventional linear FB control strategies, friction-model-based FF friction compensation approaches, etc, which are highly suitable for industrial applications.

As the future challenges, further improved command shaping approaches such as infinite-impulse-response (IIR)-type command shaping filter design, optimal command shaping considering the FB control property, learning-based command shaping, etc., will be studied on the basis of the overshoot suppression strategy presented in this paper.

Acknowledgment

The authors would like to thank Via Mechanics, Ltd, for supporting experimental equipment.

References

[1] F. Al-Bender and J. Swevers, Characterization of friction force dynamics, IEEE Contr. Syst. Mag., vol.28, no.6, pp.64–81, 2008.
[2] T. Oomen, Advanced motion control for precision mechatronics: control, identification, and learning of complex systems, IEEJ Journal Ind. App., vol.7, no.2, pp.127–140, 2018.
[3] Y. Maeda and M. Iwasaki, Feedforward friction compensation using the rolling friction model for micrometer-stroke point-to-point positioning motion, IEEJ Journal Ind. App., vol.7, no.2, pp.141–149, 2018.
[4] Z. Jamaludin, H.V. Brussel, and J. Swevers, Friction compensation of an XY feed table using friction-model-based feedforward and an inverse-model-based disturbance observer, IEEE Trans. Ind. Electron., vol.56, no.10, pp.3848–3853, 2009.
[5] H. Asaumi and H. Fujimoto, Proposal on nonlinear friction compensation based on variable natural length spring model, in Proc. 2008 SICE Annu. Conf., pp.2393–2398, 2008.
[6] T. Takemura and H. Fujimoto, Proposal of novel rolling friction compensation with data-based friction model for ball screw driven stage, in Proc. 36th Annu. Conf. IEEE Ind. Electron. Society, pp.1932–1937, 2010.
[7] Y. Maeda and M. Iwasaki, Initial friction compensation using rheology-based rolling friction model in fast and precise positioning, IEEE Trans. Ind. Electron., vol.60, no.9, pp.3865–3876, 2013.
[8] L. Roveda, G. Pallucca, N. Pedrocchi, F. Braghin, and L.M. Tosatti, Cartesian tasks oriented friction compensation through a reinforcement learning approach, in Proc. 2016 IEEE Conf. Adv. Intelligent Mechatron., pp.895–900, 2016.
[9] B.D. Bui and N. Uchiyama, Sliding mode contouring controller design with adaptive friction compensation for three-axis machine tools, in Proc. 2016 American Control Conf., pp.2217–2222, 2016.
[10] N. Hirose, M. Iwasaki, M. Kawafuku, and H. Hirai, Deadbeat feedforward compensation with frequency shaping in fast and precise positioning, IEEE Trans. Ind. Electron., vol.56, no.10, pp.3790–3797, 2009.